TgCRND8 Amyloid Precursor Protein Transgenic Mice Exhibit an Altered γ-Secretase Processing and an Aggressive, Additive Amyloid Pathology Subject to Immunotherapeutic Modulation†

Gregory D. Van Vickle,‡ Chera L. Esh,‡ Walter M. Kalback,‡ R. Lyle Patton,‡ Dean C. Luehrs,‡ Tyler A. Kokjohn,‡,§ Frederick G. Fifield,|| Paul E. Fraser,⊥ David Westaway,⊥ Joanne McLaurin,⊥ John Lopez,▽ Daniel Brune,▽ Amanda J. Newel,○ Marissa Poston,○ Thomas G. Beach,○ and Alex E. Roher*,‡

The Longtine Center for Molecular Biology and Genetics and W. H. Civin Laboratory of Neuropathology, Sun Health Research Institute, Sun City, Arizona 85351, Department of Microbiology, Midwestern University, Glendale, Arizona 85308, Pathology Section, Sun Health Boswell Hospital, Sun City, Arizona 85851, Centre for Research in Neurodegenerative Diseases, University of Toronto, Ontario M5S 3H2, Canada, and Department of Chemistry and Biochemistry, Arizona State University, Tempe, Arizona 85287

Received May 17, 2007; Revised Manuscript Received July 11, 2007

ABSTRACT: We investigated the morphology and biochemistry of the amyloid-β (Aβ) peptides produced in TgCRND8 Tg mice carrying combined amyloid precursor protein (APP) Swedish (K670M/N671L) and Indiana (V717F) mutations. Histological analyses employing amyloid-specific staining and electron microscopy revealed that the TgCRND8 Tg mice produce an aggressive pathology, evident as early as 3 months of age, that is a composite of core plaques and peculiar floccular diffuse parenchymal deposits. The Aβ peptides were purified using combined FPLC−HPLC, Western blots, and immunoprecipitation methods and characterized by MALDI-TOF/SELDI-TOF mass spectrometry. The C-terminal APP peptides, assessed by Western blot experiments and mass spectrometry, suggested an alteration in the order of secretase processing, yielding a C-terminal fragment pattern that is substantially different from that observed in sporadic Alzheimer's disease (AD). This modified processing pattern generated longer Aβ peptides, as well as those ending at residues 40/42/43, which may partially explain the early onset and destructive nature of familial AD caused by APP mutations. Despite an aggressive pathology that extended to the cerebellum and white matter, these animals tolerated the presence of an imposing amount of Aβ load. Aβ immunization resulted in an impressive 7-fold reduction in the number of amyloid core plaques and, as previously demonstrated, a significant memory recovery. However, given the phylogenetic distance and the differences in APP processing and Aβ chemistry between Tg mice and AD, caution should be applied in projecting mouse therapeutic interventions onto human subjects.

Alzheimer's disease (AD)[1] is the most prevalent form of dementia and is ranked fourth in causes of death among the elderly. In the United States, AD presently affects about 4 million individuals. It has been estimated that by the year 2050 the number of AD patients will be quadrupled (*1*). The profuse accumulation of amyloid fibrils in the brain parenchyma and cerebrovascular walls, a neuropathological hallmark of AD, lends strong support to the amyloid cascade hypothesis as an explanation for the underlying etiology of this disease (*6*). The amyloid hypothesis is further bolstered by familial cases of AD in which several mutations in the amyloid precursor protein (APP) gene result in an accelerated amyloid deposition and dementia. However, in AD other potential pathogenetic factors such as chronic brain hypoperfusion and a breakdown in brain energy metabolism mediated by cardiovascular and cerebrovascular disease (*8*, *31*) may be primary events responsible for irreversible neuronal injury and amyloid-β (Aβ) overproduction (*19*, *29*).

† This study was supported by The National Institute on Aging (Grant RO1 AG 19795), The Arizona Alzheimer's Disease Core Center (Grant P30 AG-19610), The State of Arizona Alzheimer's Disease Research Consortium, The Canadian Institutes for Health Research, The Alzheimer Society of Ontario, The Ontario Mental Health Foundation, and The Natural Science and Engineering Research Council of Canada.

* To whom correspondence should be addressed. Phone: (623) 876-5465. Fax: (623) 876-5698. E-mail: alex.roher@sunhealth.org.

‡ The Longtine Center for Molecular Biology and Genetics, Sun Health Research Institute.

§ Midwestern University.

|| Sun Health Boswell Hospital.

⊥ University of Toronto.

▽ Arizona State University.

○ W. H. Civin Laboratory of Neuropathology, Sun Health Research Institute.

[1] Abbreviations: Aβ, amyloid-β; AD, Alzheimer's disease; AICD, APP intracellular domain; APP, amyloid precursor protein; CHCA, α-cyano-4-hydroxycinnamic acid; CT, carboxy-terminal; DTT, dithiothreitol; FPLC, fast-performance liquid chromatography; GDFA, glass-distilled formic acid; HPLC, high-performance liquid chromatography; HRP, horseradish peroxidase; IAPP, islet-associated polypeptide; IP, immunoprecipitation; MALDI-TOF, matrix-assisted laser desorption/ionization time-of-flight; ND, nondemented; NFTs, neurofibrillary tangles; PBS, phosphate-buffered saline; PrP, hamster prion; PS, presenilin; rt, room temperature; SELDI-TOF, surface-enhanced laser desorption/ionization time-of-flight; TEM, transmission electron microscopy; TFA, trifluoroacetic acid; Tg, transgenic.

10.1021/bi700951u CCC: $37.00
Published on Web 08/18/2007

Proteolytic degradation of the APP molecule by β- and γ-secretases generates peptides 40−42 amino acids long. These Aβ peptides compose the amyloid deposits. The N-terminal domain of Aβ is made of 28 mostly hydrophilic amino acids, while the Aβ C-terminal domain contains 12−14 hydrophobic amino acid residues, partially representing the APP transmembrane domain. Once extruded from the membrane, the metastable amphipathic Aβ peptides associate into insoluble fibrillar polymers or into soluble oligomeric structures that have toxic effects on brain and vascular cells (*15*, *30*, *36*, *39*).

Several transgenic (Tg) mouse models have been constructed (*5*) that express human familial AD APP mutations and produce massive amyloid deposition with cognitive and memory disturbances. To hasten the onset of amyloid deposition and enhance amyloid load and behavioral changes, double Tg mice have been generated that combine APP and presenilin (PS) mutations. PS1 and PS2 apparently contain the active center of the γ-secretase (*38*). More recently, a triple-Tg mouse has been designed by combining the APP (K670M/N671L) mutation, the PS1 (M146V) mutation, and the tau (P301L) mutation, which produces intracellular neurofibrillary tangles (NFTs), the second neuropathological marker of AD, as well as amyloid deposits (*27*).

We investigated the chemical nature of the Aβ peptides produced by TgCRND8 Tg mice carrying combined APP Swedish (K670M/N671L) and Indiana (V717F) mutations that result in early-onset amyloid deposits which are obvious as early as 3 months of age (*3*). Immunization of the TgCRND8 Tg mice against Aβ42 produced a significant memory recovery along with a patent diminution in the number of amyloid plaque deposits. However, the total amount of formic acid-extractable Aβ did not decrease, suggesting that the Aβ mobilized from plaque deposits was not cleared from the brain (*10*). To assess the relative merits and limits of the APP Tg mouse strains as both AD pathology models and potential immunotherapy evaluation tools, we have compared amyloid morphology and chemistry among the different strains of APP Tg mice with those characteristically observed in sporadic AD patients.

MATERIALS AND METHODS

APP TgCRND8 Transgenic Mice. This strain of Tg mice was developed by the Centre for Research in Neurodegenerative Diseases of the University of Toronto (*3*). The APP transcript encodes the double mutant of the APP_{695} isoform carrying the Swedish mutations, K670M/N671L, and the Indiana mutation, V717F (both mutations described in the APP_{770} isoform amino acid notation), under the control of the hamster prion (PrP) gene promoter. The animals were maintained on a C3H/B6 outbred background. Thioflavin-S-positive deposits are typically present at 3 months of age, with dense core plaques and neuritic pathology evident from 5 months of age. The TgCRND8 mice exhibit between 3.2 and 4.6 ng of Aβ42/g of brain at 6 months of age, with an excess of Aβ42 over Aβ40 (*3*). In this strain of Tg mice, by 3 months of age, the level of production of human Aβ peptides is associated with an impairment in acquisition and learning reversal in the reference memory version of the Morris water maze (*3*).

Histological Assessment. To determine the extension of amyloid accumulation, 6 μm sagital sections were prepared from whole TgCRND8 Tg mouse brains and stained using Campbell−Switzer silver stain and thioflavin-S. A whole brain photomontage was generated to obtain a global view of the amyloid load in different parts of the mouse brain. Transmission electron microscopy (TEM) was employed to assess the ultrastructural aspects of the plaques. Vibratome sections were probed with anti-Aβ monoclonal antibody 6E10 (Signet Laboratories, Dedham, MA) and amyloid plaques visualized by HRP-conjugated secondary antibodies. Areas rich in amyloid plaques were dissected from the sections and postfixed with 2.5% glutaraldehyde in 0.1 M sodium cacodylate buffer at 4 °C followed by treatment with osmium tetroxide. Dehydrated tissues were embedded in epoxy resin and processed for ultrathin sectioning. Stained sections were visualized in a Hitachi H-7000 operating with an accelerating voltage of 75 kV. Negative-staining TEM was performed using carbon-coated grids that were floated on aqueous solutions of Aβ peptides; the grids were blotted, air-dried, and stained with 1% phosphotungstic acid and examined on a Hitachi H-7000 transmission electron microscope as described above.

Whole-mount preparations from leptomeningeal and cerebral arteries were prepared to assess the vascular amyloid load. The separated cerebral hemispheres from five TgCRND8 Tg mice, 7 months old, were stirred for 36 h in 200 mL of 0.1 M Tris−HCl buffer, pH 7.5, containing 3% SDS. The insoluble tufts of blood vessels were recovered by filtration through a 25 μm nylon mesh and the vessels removed by shaking the mesh in 200 mL of water, subsequently pelleted at 2000*g*, and washed two times under the same conditions. The samples were spread on slides, dried at 65 °C, and stained by thioflavin-S. In searching for SDS-insoluble amyloid cores, the 3% SDS supernatant from the vessel preparation was centrifuged at 250000*g* for 4 h at 21 °C, and the resulting pellets were spread on a microscope slide, air-dried, fixed with absolute ethanol, and stained with thioflavin-S.

Assessment of Aβ Vaccination on TgCRND8 Tg Mice. The brain histological effects of Aβ immunization were evaluated on a set of three TgCRND8 Tg mice. In this active immunization test the antigen consisted of the human Aβ 1−42 sequence in β-sheet conformation and in fibrillar form (assessed by circular dichroism and by TEM). Mice entered the experiment between 42 and 70 days of age, prior to the first appearance of CNS amyloid deposits. The mice were vaccinated with antigen doses of 100 μg in 100 μL in Freund's adjuvant. Subsequent vaccinations at 14, 42, 84, and 112 days later also contained the same doses and volumes but were prepared in incomplete Freund's adjuvant. The mice described here were euthanized at 180, 185, and 202 days of age. At the time of vaccination, the Aβ42 and control islet-associated polypeptide (IAPP; Bachem, Torrance, CA) were in β-pleated-sheet conformation. Initial Aβ42 antibody titers in Aβ42-immunized mice were measured by ELISA (*37*) at 91 days of age: 1:(3640 $\pm$ 470). The antibody titers at 161 days increased to 1:(7500 $\pm$ 1712).

To assess the effects of Aβ vaccination, a group of three non-Aβ-vaccinated TgCRND8 Tg mice of matching ages were used as controls. Complete sagital sections (6 μm thick) of the mouse brains were stained by thioflavin-S and the Campbell−Switzer silver technique and the total number of

core amyloid plaques counted on three sections per vaccinated and unvaccinated control TgCRND8 Tg mouse.

Extraction and Enrichment of Aβ and APP-Related Peptides by Fast Protein Liquid Chromatography (FPLC) and High-Performance Liquid Chromatography (HPLC). For the present biochemical experiments, the frozen brains from 20 TgCRND8 Tg mice ranging from 9 to 19 months of age were utilized. The brain stem and cerebellum were separated from the brain and the cerebrum, representing 3.5 g of total wet tissue, finely minced, and thoroughly homogenized in 40 mL of 90% glass-distilled formic acid (GDFA; distilled in our laboratory). The homogenate was loaded into polyallomer tubes and centrifuged at 250 000*g* for 1 h at 5 °C, using an SW 41 rotor (Beckman Coulter, Fullerton, CA). The compact lipid-containing layer at the top of the centrifuge tubes and the acid-insoluble pellet were carefully avoided, and the clear supernatant was fractionated into 75 samples, 500 μL each, which were stored at −80 °C. Each of these specimens was submitted to FPLC (Amersham Biosciences/GE, Piscataway, NJ), using a 500 μL loading loop, on a Superose 12 size-exclusion column (10 mm × 300 mm, Biosciences/GE). The Superose 12 columns were calibrated using a peptide composed of Aβ amino acid residues 40−1 synthesized in reverse order (California Peptide Inc., Napa, CA). FPLC was equilibrated and developed at a flow rate of 15 mL/h at room temperature and monitored at 280 nm. The eluate containing the 2−8 kDa peptides was collected in polypropylene tubes (to reduce adsorption of Aβ peptides) containing 5 μL of 10% betaine to prevent Aβ aggregation. The volume of the specimens was reduced to 100 μL by vacuum centrifugation (Speedvac, Savant Instruments Inc., Farmingdale, NY). To enhance the separation and elimination of the flanking contaminating fractions, two of the FPLC 2−8 kDa fractions were pooled, their volume reduced, and the fractions rechromatographed by FPLC under the same conditions. The volume of eluate, containing the 2−8 kDa protein fractions, was reduced to 50 μL as stated above. The FPLC Aβ fractions were brought to 100 μL volume with 80% GDFA and loaded onto two size-exclusion silica-based Synchropak GPC-peptide columns connected in series (600 mm × 7.8 mm and 300 mm × 7.8 mm, total bed 1000 mm × 7.8 mm; Synchrom, Inc., Lafayette, IN). Chromatography was developed in 80% GDFA formic acid at a flow rate of 0.2 mL/min at room temperature and monitored at 280 nm. Western blot analyses were performed to locate the Aβ peptides using polyclonal antibodies against the C-terminal region of Aβ 40 and Aβ 42 (Biosource, Camarillo, CA). The Aβ fractions were pooled from two GPC-peptide chromatographies, reduced to ∼100 μL, followed by the addition of 200 μL of 80% GDFA and 200 μL of water, and applied to an HPLC system (Thermo Separation Products/Finnigan Corp., Fremont, CA), using a 500 μL loading loop. Chromatography was resolved on a reversed-phase Zorbax SB-C8 column (250 mm × 4.6 mm; Agilent Technologies, Palo Alto, CA) using a 60 min linear gradient from 20% to 40% acetonitrile in water containing 0.1% trifluoroacetic acid (TFA) at a flow rate of 0.8 mL/min at 80 °C constant temperature and monitored at 214 nm. We further investigated the proteins contained in the 100% acetonitrile push used to clean the column after the end of the 40% acetonitrile gradient. This material was rechromatographed on the Zorbax SB-C8 column under the same conditions as stated above but using a linear gradient from 38% to 60% acetonitrile in water/0.1% TFA.

Assessment of Aβ and APP Peptides by Western Blot. Brain tissue was homogenized in 10 volumes of PBS solution, pH 7.4, containing complete protease inhibitor cocktail (Roche Diagnostics, Mannheim, Germany). Total protein concentrations were quantified using the BCA protein assay kit (Pierce, Rockford, IL). Samples were combined with NuPage LDS sample buffer (Invitrogen, Carlsbad, CA) containing 50 mM dithiothreitol (DTT) and heated to 80 °C for 10 min. Equal amounts of protein were loaded onto 4−12% Bis-Tris gels (Invitrogen) and electrophoresed using NuPage MES running buffer. Kaleidoscope prestained protein molecular mass standards (Bio-Rad, Hercules, CA) were run on each gel. Proteins were electroblotted onto nitrocellulose membranes (Invitrogen) using NuPage transfer buffer containing 20% methanol. The membranes were blocked in 5% nonfat dry milk in phosphate-buffered saline (PBS) and 0.5% (v/v) Tween-20 (Fluka, St. Louis, MO). Carboxy-terminal proteins were detected with a 1:1500 dilution of an antibody raised against the last nine amino acids of APP (Chemicon International, Temecula, CA; heretofore designated as CT9APP) and with the CT 369 antibody raised against the last 50 amino acids of the APP (kindly provided by Dr. Sam Gandy). Aβ peptides were detected with the anti-Aβ 40 (0.5 μg/mL) and anti-Aβ 42 (0.5 μg/mL) (Biosource). Bound primary antibodies were detected with a 1:10000 dilution of goat anti-rabbit horseradish peroxidase (HRP)-conjugated secondary antibody from Pierce. The Western blots were developed with SuperSignal West Pico chemiluminescent substrate and CL-Xpose film (Pierce) and Kodak GBX developer. All films were scanned using a GS-800 calibrated densitometer (Bio-Rad).

Immunoprecipitation of APP C-Terminal Peptides. Samples from the formic acid-soluble 2−8 kDa FPLC fraction obtained from TgCRND8 Tg mouse brains were subjected to immunoprecipitation (IP). Formic acid was removed by drying under speed vacuum, and the samples were suspended in 100 μL of distilled water. This procedure was repeated three times and the resultant pellet suspended in 1 mL of IP buffer: 30 mM Tris−HCl, pH 8, 140 mM NaCl containing 0.1% Triton X-100 and complete protease inhibitor cocktail (Roche Diagnostics). Nonspecific cross-reacting material was adsorbed by incubation with 5 μL of normal rabbit serum and Ultralink immobilized protein A beads (Amersham Biosciences/GE) for 16 h at 4 °C followed by centrifugation at 3500 rpm for 5 min in an Eppendorf microfuge. The pellet was discarded and the supernatant incubated overnight at 4 °C with rabbit antibody 369 raised against the 50 C-terminal amino acids of APP and 90 μL of protein A bead slurry in IP buffer. After being washed three times with IP buffer and three times with 10 mM Tris−HCl, pH 8, the immunoprecipitates were suspended in an equal volume of NuPage LDS sample buffer (Invitrogen) containing 0.1 M DTT and boiled for 10 min. The proteins were analyzed by SDS−PAGE and Western blot using CT9APP and 369 antibodies as described in the previous section.

MALDI-TOF Mass Spectrometry of Aβ and APP-Related Peptides. A MALDI-TOF Voyager DE STR mass spectrometer (Applied Biosystems, Foster City, CA) fitted with a nitrogen laser that generated 337 nm pulses of 3 ns duration at a repetition rate of 20 Hz was used to acquire data in the

positive mode employing delayed extraction and a reflectron. The HPLC fractions were reduced to ~30 μL. A 5 μL portion of the sample was added to 5 μL of a saturated solution of α-cyano-4-hydroxycinnamic acid (CHCA) dissolved in 50% acetonitrile/0.1% TFA. Aliquots of 0.5 μL were spotted on a sample plate and mass spectra obtained by averaging 100 laser shots. Calibration was made using the CalMix 2 mixture (Applied Biosystems). The detailed composition of the calibration markers is presented elsewhere (*4*).

SELDI-TOF Mass Spectrometry. Selected HPLC peaks were dialyzed with 1000 MW cutoff bags against PBS, pH 8, twice for 1 h intervals. The dialyzed peptide samples were analyzed using SELDI-TOF (surface-enhanced laser desorption/ionization time-of-flight) mass spectrometry (Ciphergen Biosystems, Freemont, CA). The monoclonal and polyclonal antibodies MAB343 (Chemicon International) and 369, respectively, were purified using HiTrap protein G HP affinity columns (Amersham Biosciences/GE). PS20 ProteinChip arrays were prepared by loading 4 μL of PBS onto the chip spots and incubating for 15 min at room temperature (rt). The purified antibodies were adjusted to a concentration of 0.5 mg/mL in PBS, loaded (4 μL) onto PS20 chip arrays, and incubated in a humidity chamber for 1 h at rt. The chip surfaces were blocked with 4 μL of ethanolamine (1 M, pH 8) for 30 min. The sample spots were individually washed once with 4 μL of PBS + 0.5% (v/v) Triton X-100 and twice with 4 μL of PBS. The protein chips were loaded with either 4 μL of sonicated sample or 4 μL of the synthetic APP C-terminal peptide 770 (residues 732−751) (Bachem) as a positive control and incubated overnight at 4 °C. After the sample binding solutions were removed, the spots were individually washed twice with 4 μL of PBS + 0.5% (v/v) Triton X-100, once with 4 μL of PBS, and once with 4 μL of distilled water. The chips were then air-dried, a 1:5 dilution of saturated CHCA in 50% acetonitrile with 0.1% TFA was applied two times (0.5 μL), and mass assignments were made by 100 averaged shots in a Ciphergen SELDI Protein Biology System II. Calibration was made externally using the Ciphergen All-In-1 peptide standard.

Synthesis of Aβ peptides. Amyloid-β peptide (Aβ 1−47) was synthesized by solid-phase Fmoc chemistry by The Hospital of Sick Children's Biotechnology Centre (Toronto, Ontario, Canada). The Aβ peptide was purified by HPLC reversed-phase chemistry on a C18 M-Bondapak column using a 0−60% acetonitrile/0.1% TFA gradient. The peptide was allowed to polymerize for a period of 7 days in distilled water at 37 °C. The aggregated Aβ was negatively stained and observed on a transmission electron microscope as described above.

RESULTS

Morphological analysis of the TgCRND8 Tg mouse brain demonstrates that deposition of amyloid core plaques and floccular Aβ deposits starts at about 3 months of age. By 9−11 months there is a severe deposition, and by 14−17 months the number of amyloid plaques is overwhelming, involving all areas of the brain including the white matter and cerebellum (Figure 1A). Examination of the abundance of amyloid core plaques and flocculent deposits in young Aβ-immunized and nonimmunized TgCRND8 Tg mice demonstrated a dramatic reduction of amyloid deposition at approximately 3 months post-Aβ vaccination (Figure 1B,C, respectively). The average number of thioflavin-S-positive amyloid core plaques, per sagital section of the cerebrum, in the immunized animals was 62 (n = 3), while in nonimmunized matching age mice (n = 3) the mean value was 425, a significant 7-fold difference. Even more impressive was the remarkable absence of flocculent, Campbell−Switzer-positive, Aβ deposits which are very abundant in the 6−7 month old nonvaccinated TgCRND8 Tg mice. These outstanding changes in the numbers of plaques in immunized Tg mice were accompanied by a moderate increase in vascular amyloid deposition mostly observed in leptomeningeal vessels (Figure 1D).

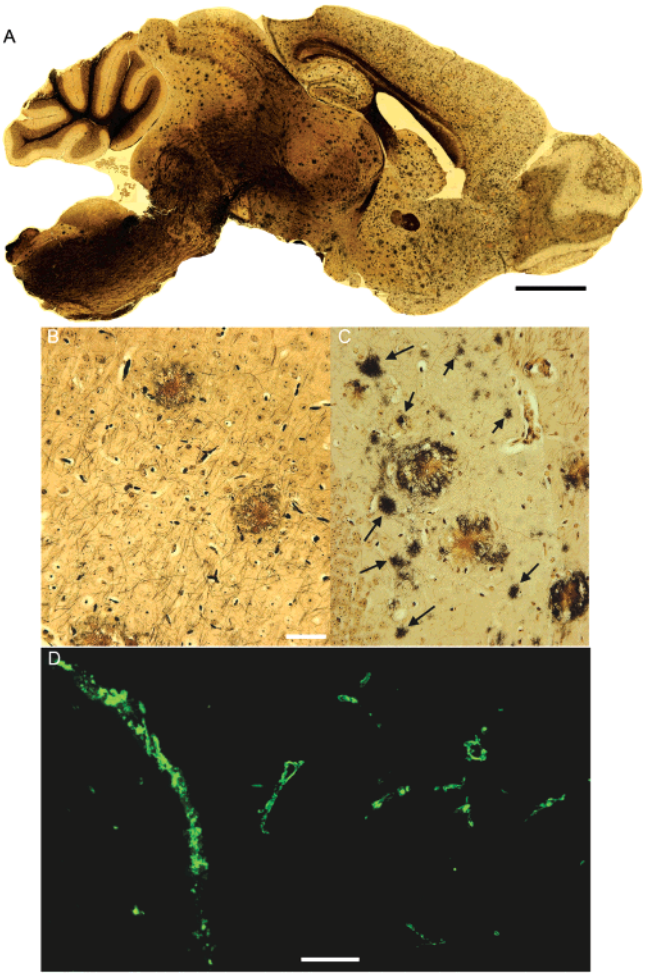

FIGURE 1: Campbell−Switzer silver- and thioflavin-S-stained sections of unimmunized and immunized TgCRND8 Tg mice. (A) The section demonstrates abundant amyloid core plaques intermingled with a vast number of floccular plaques in a 17 month old Tg mouse. The former are stained in brown-orange color, while the latter are black. In many instances, the plaques coalesce to generate large conglomerates or are deposited in a profuse tapestry of small, punctuated spots that appear, at low magnification, like powdery material. Both types of plaques are found in the cerebral cortex, white matter, hippocampus, superior and inferior colliculi, corpus callosum, olfactory bulbs, striatum, thalamus and hypothalamus, midbrain, and pons and medulla oblongata. Although not visible at this magnification, the cerebellum of the TgCRND8 Tg mouse contains numerous amyloid core plaques. (B, C). These sections correspond to 7 month old Aβ-immunized and unimmunized mice, respectively. Notice that in the latter there are numerous floccular plaques (arrows) that are not present in the former. (D) In the 7 month old Aβ-immunized mouse there is a moderate increase in cerebrovascular amyloidosis mainly localized at the leptomeningeal arteries. Scale bars: A, 1 mm; B, C, D, 50 μm.

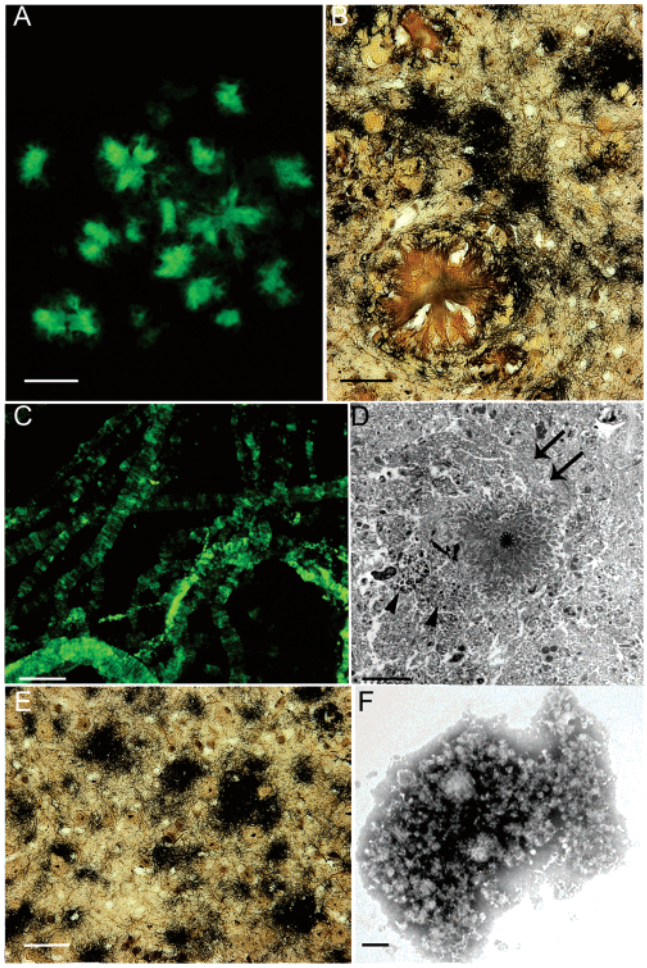

FIGURE 2: Amyloid deposition in a 17 month old TgCRND8 Tg mouse. (A) A group of amyloid core plaques stained by thioflavin-S. The amyloid core plaques are spherical structures with radiating wisps of amyloid fibrils that are positive for thioflavin-S. The fluorescent fibrils radiate from the center, giving the impression of a stellar configuration with brushlike borders. (B) Large amyloid core plaque stained in brown-orange color with the Campbell−Switzer silver technique. As time elapses the cores are surrounded with black floccular plaque deposits. (C) An air-dried whole montage of isolated leptomeningeal and cortical vessels stained by thioflavin-S. At 17 months of age, the load of vascular amyloid is severe. The deposits adopt a ringlike pattern perpendicular to the main axis of the vessel and parallel to the orientation of the smooth muscle cells. (D) Transmission electron micrograph showing a central core of amyloid (asterisk) surrounded by dystrophic neurites filled with multilamellar bodies and dense bodies (arrowheads). Just above the amyloid core there is a confluent floccular deposit (arrows). (E) The floccular deposits become the most abundant Aβ in older Tg mice. These aggregates are negative for thioflavin-S and are mainly composed of elongated Aβ peptides. (F) Uranyl acetate negative staining preparation of an Aβ 1−47 synthetic peptide aggregate made of an amorphous conglomerate of molecules suggesting a supercoiled structure. Scale bars: A, 50 μm; B, 25 μm; C, 100 μm; D, 25 μm; E, 25 μm; F, 100 nm.

In the TgCRND8 Tg mice, microscopic observations demonstrated that the Aβ plaques corresponded to two remarkably different types: core plaques and floccular deposits. In many instances the amyloid core plaques form aggregates of many confluent starlike plaques in the cerebrum and cerebellum (Figure 2A). These intensely thioflavin-S-positive starlike plaques, which were stained light brown with the silver technique (Figure 2B), coexist with thioflavin-S-negative deposits made of diffuse amorphous reticular

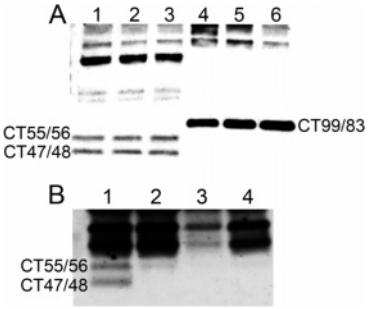

FIGURE 3: Western blots of brain homogenates from TgCRND8 Tg mice. (A) Brain homogenates were immunoreacted with the CT9APP antibody raised against the last nine C-terminal amino acids of APP. Lanes 1, 2, and 3 correspond to Tg mice 8, 5, and 7 months of age, respectively. Lanes 4 and 5 originated from two sporadic AD patients ages 72 and 78 years old, respectively. Lane 6 represents an ND 73 year old patient. The human specimens were Apo E 3/3, Apo E 3/4, and Apo E 3/4, respectively. Notice that between the Tg mice and human specimens there are remarkable differences in the M_r of the C-terminal peptides. The human produced the CT99 and CT83 species, which overlap in the present SDS−PAGE system, while the Tg mice generated two CT bands with a lower $M_r \approx 5000-7000$ that corresponds to CT55/56 and CT47/48. In addition, the Tg mice had C-terminal peptides with an approximate M_r of 35 000 that are absent in the human specimens. (B) To corroborate the nature of the C-terminal peptides, the Tg mouse soluble fraction was immunoprecipitated with antibodies against the last 50 C-terminal amino acids of APP (antibody 369) and probed with the last 9 C-terminal amino acids of APP (antibody CT9APP): lane 1, HPLC peaks 6 and 7 (from Figure 5E); lane 2, 50 μg of CT APP 22 kDa standard, positive control; lane 3, HPLC peaks 6 and 7 (from Figure 5E) plus rabbit vascular epithelium growth factor antibody, negative control; lane 4, 50 μg of bovine serum albumin, negative control.

material, the type that we previously defined as floccular Aβ deposits (*4*, *32*). These deposits are intensely dyed in black color by the Campbell−Switzer silver stain (Figure 2B,E). As age advances, the floccular deposits become confluent in many areas of the brain. Electron microscopy demonstrated the radial disposition of the amyloid bundles in the core plaques which are surrounded by dystrophic neurites filled with dense bodies made of degenerating membranes. In addition, the plaques are also associated with floccular diffuse deposits of Aβ peptides (Figure 2D). These latter deposits are made of nonfibrillar Aβ which extends beyond Aβ residue 42 (vide infra). Synthetic Aβ 1−47 generates nonfibrillar peptide aggregates that at the electron microscope level resemble those observed in the diffuse floccular Aβ deposits (Figure 2F).

Accompanying the plaque core and floccular pathology is a moderate degree of cerebrovascular amyloidosis of the leptomeningeal and gray matter arteries that also starts at 3 months of age. The typical cross-striated vascular amyloid deposits observed in the TgCRND8 Tg mice are shown in Figure 2C. Thioflavin-S fluorescence and silver staining did not reveal the presence of neurofibrillary tangles or neuropil threads commonly seen in familial and sporadic AD.

In humans with sporadic AD or nondemented (ND) individuals, Western blots probed with antibodies raised against the C-terminal (CT) domains of APP reveal the presence of the APP CT fragments CT99 and CT83 (Figure 3A). Intriguingly, in the TgCRND8 Tg mice carrying the Swedish and Indiana mutations (K670M/N671L and V717F), the CT99 and CT83 bands were absent while there were two prominent CT bands at approximately 5 and 7 kDa that were

Table 1: CT APP Peptides Identified by MALDI-TOF and SELDI-TOF Mass Spectrometry in TgCRND8 Tg Mice[a]

	obsd mass (Da)	calcd mass (Da)	peptide fragment	modification
MALDI-TOF	6625.59	6625.59	44−99	F
	6646.15	6645.59	44−99	3O
	6740.20	6741.59	44−99	4F + 2O
	6603.44	6602.45	45−99	2F + 3O
	6625.59	6626.45	45−99	4F + O
	5713.19	5712.37	52−99	2O
	5753.62	5752.37	52−99	2F + O
	5713.19	5711.21	53−99	4F + O
SELDI-TOF	6599.56	6597.59	44−99	
	6614.32	6613.59	44−99	O
	6627.98	6625.59	44−99	2O
	6642.07	6641.59	44−99	F + O
	6569.50	6570.45	45−99	2F + O
	5685.94	5687.21	53−99	2F + 4O
	5441.69	5442.86	54−99	
	5469.91	5471.01	54−99	2O

[a] F = formylation of Ser and/or Thr residues; O = oxidation of Met residues.

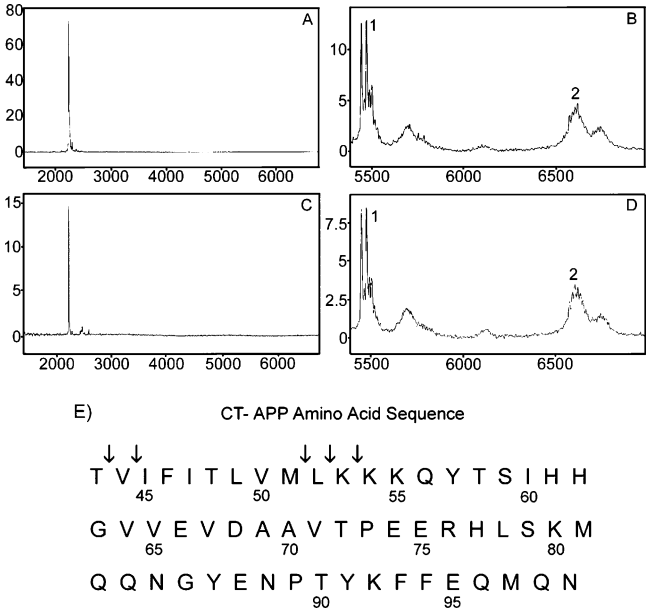

FIGURE 4: SELDI-TOF mass spectra of the CT APP peptides from the TgCRND8 Tg mouse APP. (A, C) Positive controls in which the APP 369 and the APP 343 antibodies, respectively, were used to capture the synthetic peptide residues 732−751 of APP_{770}. (B, D) Mass spectra of the Tg mouse CT APP peptides captured by 369 and 343 antibodies, respectively. Cluster 1 corresponds to the CT APP peptide residues 53−99 and 54−99. Cluster 2 corresponds to the CT APP peptide residues 44−99 and 45−99 (all given in the Aβ sequence). (E) Amino acid sequence of the C-terminal region of APP_{695} comprising residues 640−695. The amino acid notation given in this figure corresponds to the continuation of the Aβ peptide sequence from Aβ 43 (=APP_{695} residue 640) to Aβ 99 (=APP_{695} residue 695). The arrows indicate hydrolysis at the C-side of Aβ sequence of residues 43, 44, 51, 52, and 53, yielding APP CT55/56 and CT47/48.

absent in the human sporadic AD and ND controls (Figure 3A). We suggest that these low-M_r molecules correspond to the chromatographically recovered APP CT fragments, detected by the CT9APP and 369 antibodies raised against the last 9 and 50 amino acid residues of APP, respectively. MALDI-TOF mass spectrometry indicated that the APP CT peptides were composed of residues 44−99 and 45−99 ($M_r \approx 6600$, henceforth designated as TC55/56) and the shorter APP CT peptides 52−99 and 53−99 ($M_r \approx 5700$, henceforth designated as CT47/48) (Table 1, sequences given in Aβ amino acid notation). To demonstrate the chemical nature and to further purify the APP CT peptides, immunoprecipitation was performed using the 369 antibody. The captured peptides were analyzed by Western blot (Figure 3B) using the CT9APP antibody, which confirmed the presence of both CT low-M_r peptides seen in the crude brain homogenates (Figure 3A). To more definitely confirm the chemical nature of the shorter APP CT peptides, we used the 369 and the MAB 343 antibodies (raised against the last 52 amino acids of APP; Chemicon International) as capture antibodies for SELDI-TOF mass spectrometry. This step demonstrated the presence of CT peptides with N-termini at residues 44, 45, 53, and 54 and a C-terminus at residue 99. The mass spectra of these peptides are shown in Figure 4 and Table 1, which in addition depicts the amino acid sequence of APP respective CT domains (Figure 4E). These APP CT peptides probably represent alternative byproducts of the γ-secretase and/or the result of as yet to be determined endopeptidase(s).

To ensure a thorough analysis of the mouse Aβ peptides, we homogenized the Tg mouse brains in 80% GDFA, a treatment that solubilizes all types of amyloid deposits, and performed a high-speed ultracentrifugation to separate insoluble lipids and pellets. The acid-soluble molecules were submitted to FPLC, and the Aβ-containing fractions were collected (Figure 5A) and further purified by HPLC size-exclusion chromatography (Figure 5B). Western blot analysis revealed those peaks harboring the Aβ peptides (data not shown), which were concentrated and submitted to high-temperature C8 reversed-phase HPLC separation with an acetonitrile gradient as the mobile phase (Figure 5C). A Western blot using antibodies against Aβ 40 and Aβ 42 demonstrated the presence of Aβ monomeric and oligomeric peptides (Figure 5D). After the end of the gradient (40% acetonitrile), the column was flushed with 100% acetonitrile, and the eluted material was subjected to a second round of chromatography in the same column, using an acetonitrile linear gradient of 38−60% (Figure 5E). All the recovered fractions were tested for Aβ content by Western blot, which revealed an assortment of APP CT peptides (Figure 5F). MALDI-TOF mass spectrometry of the 12 peaks shown in Figure 5C suggested the presence of 298 Aβ-related and unmodified native Aβ peptides (Table 2). For this analysis, a small variation range of $\pm$0.8 Da was the maximum permitted when the calculated and observed masses of the Aβ-related peptides were compared. Table 2 lists these peptides in numeric order starting with the N-terminal residue. In terms of relative yield the dominant Aβ peptides contained Phe at position 46, in agreement with the high expression level of the mutated human APP transcript. Numerous peptides with oxidized Met at positions 35 and 51, both in the forms of Met-sulfoxide (additional $M_r = 16$) and Met-sulfone (additional $M_r = 32$) were detected. There were also peptides with artefactual formylation(s) of Ser and Thr residues at positions 8, 26, 43, and 48, which increase the native M_r of the peptides by 28, 56, 84, and 112. Cyclization of N-terminal Glu to yield pyroglutamyl occurred at positions 3 and 11.

A complete mass spectrometry data sheet of all 531 peptide species which includes the peptide fragment, post-translational modifications (when present), and the M_r-associated

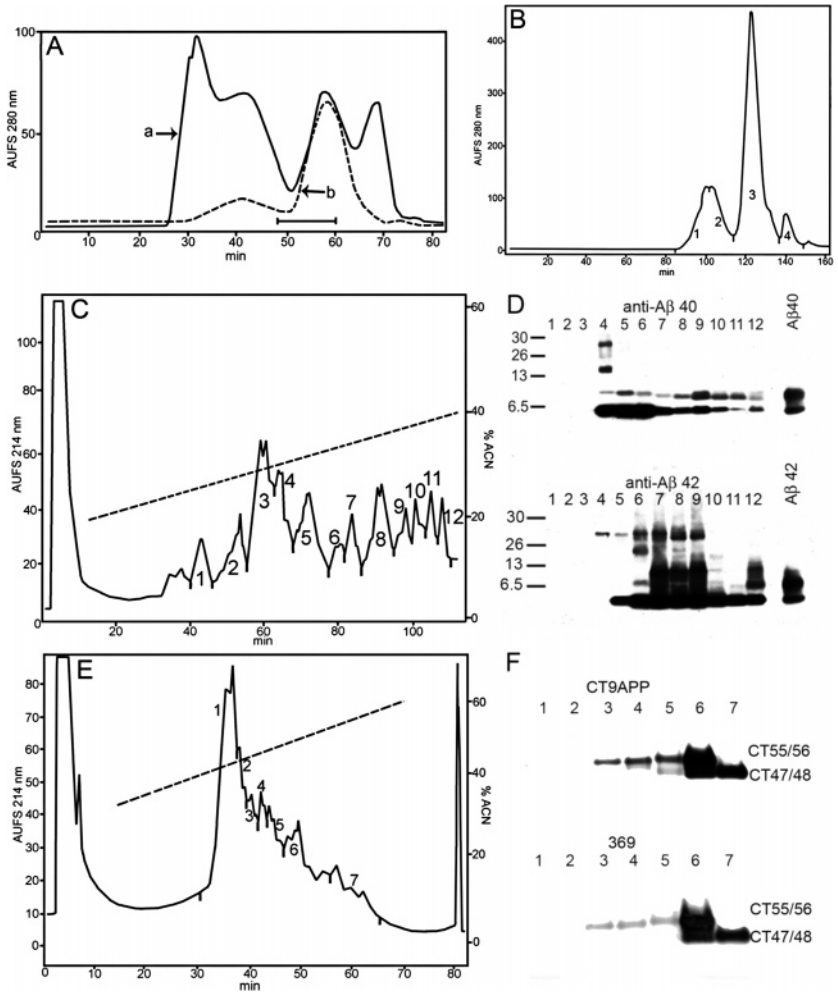

FIGURE 5: Chromatographic elution patterns of the TgCRND8 Tg mouse Aβ-related peptides. (A) Trace a indicates the Superose 12 FPLC elution profile of the acid-soluble fraction obtained from the crude brain homogenate lysed by GDFA. Trace b represents a second chromatographic step of the material indicated by the bar which was run under the same conditions to eliminate flanking contaminating proteins. (B) The material indicated by the bar in (A), containing the 2−8 kDa molecules, was separated by size exclusion HPLC on a GPC-peptide column. Western blot indicated that most of the Aβ peptides were in fractions 1 and 2 (data not shown). (C) Reversed-phase HPLC (Zorbax SB-C8 column) of the combined fractions 1 and 2 obtained from the GPC-peptide column. A total of 12 fractions were recovered, using a gradient from 20% to 40% acetonitrile concentration, and analyzed by Western blot for Aβ 40 and Aβ 42 (D). Fractions 4−12 revealed multiple Aβ-related peptides with the M_r values listed in Table 1. The 100% acetonitrile push was rechromatographed in the same column but using a gradient from 38% to 60% acetonitrile concentration. The resulting chromatographic profile is shown in (E). The recovered fractions were investigated by Western blot using the CT9APP and 369 antibodies (F). Fractions 6 and 7 contained APP C-terminal peptides CT44−99, CT45−99, CT52−99, CT53−99, and CT54−99 (numbers given in the Aβ sequence notation), whose M_r values are shown in Table 2.

chromatographic peak and relative intensity is available as Supporting Information.

Although it is not possible to deconvolute from mass spectrometry data the absolute quantities of peptides present in complex mixtures due to inherent differences in the time of flight, we estimated the average relative representations. This was accomplished by grouping Aβ peptides ending at positions 36−42, corresponding to γ-secretase hydrolysis sites, those terminating beyond residue 42, and those ending before residue 36. The estimated relative abundance of the 36−42 group of peptides was 31.19%, that of those ending between residues 43 and 53 was 33.91%, and that for those peptides ending before residue 36 was 34.90%.

DISCUSSION

The APP TgCRND8 Tg mice express an accurate biochemical composite of the Swedish and Indiana mutations to produce early and severe amyloid deposition. The individual Swedish double mutations expressed by the APP23 and the tg2576 Tg mice and the single Indiana mutation carried by the PDAPP Tg mice produced visible plaques between 8 and 11 months of age (*4*, *11*, *17*), while, in combination, the TgCRND8 deposition started at 3 months of age (*3*). Diffuse floccular and amyloid core plaques as well as vascular amyloid deposits are abundant in these mice at 6−8 months of age, an outcome only matched by the double Tg mice APP/PS1 (*2*, *18*). In contrast, in the single Tg mice APP23, tg2576, and PDAPP, similar pathologic states are observed at 20 months of age. Moreover, by 12 months of age the TgCRND8 Tg mice develop substantial cerebellar deposition of amyloid core plaques which are never seen in single APP Tg mice. Characteristic of all single APP Tg mice is the enhanced SDS solubility of the amyloid fibrils and cores compared to those present in the sporadic AD brains. Also in contrast to humans, the TgCRND8 Tg mouse amyloid fibrils present in amyloid cores completely

Table 2: Aβ-Related Peptides Found by MALDI-TOF Mass Spectrometry[a]

1−9	3−29	6−17	8−42	11PG−31	16−37	20−44	28−50 Phe
1−13	3−34	6−28	8−43	11PG−35	16−38	20−45	29−39
1−23	3−38	6−29	8−44	11PG−42	16−41	20−52 Phe	29−40
1−24	3−39	6−30	8−45	12−19	16−42	21−30	30−39
1−25	3−42	6−36	9−16	12−22	16−44	21−35	30−40
1−26	3−44	3−37	9−20	12−36	16−45	21−38	30−41
1−29	4−13	4−40	9−32	12−45	17−26	21−40	30−45
1−33	4−33	6−41	9−35	12−48 Phe	17−31	21−41	30−55 Phe
1−35	4−36	6−43	9−37	13−31	17−36	21−42	31−35
1−36	4−38	6−45	9−38	13−32	17−37	21−43	31−40
1−37	4−39	6−46 Phe	9−39	13−33	17−38	21−45	31−42
1−38	4−40	6−47 Phe	9−41	13−34	17−43	21−49 Phe	32−41
1−39	4−41	6−48 Phe	9−43	13−38	17−44	2−34	32−43
1−40	4−42	6−55 Phe	9−45	13−42	17−45	22−36	32−44
1−41	4−43	7−14	9−47 Phe	13−45	17−47 Phe	22−41	33−42
1−42	4−44	7−15	9−48 Phe	13−46 Phe	17−49 Phe	22−42	33−44
1−43	4−45	7−20	9−49 Phe	13−48 Phe	18−26	22−44	33−45
1−53 Phe	4−48 Phe	7−21	9−50 Phe	13−54 Phe	18−37	23−33	33−48 Phe
2−9	4−53 Phe	7−22	10−21	14−23	18−40	23−42	33−55 Phe
2−17	4−54 Phe	7−26	10−27	14−36	18−45	23−43	34−43
2−26	5−13	7−31	10−36	14−37	18−48 Phe	23−44	34−44
2−32	5−14	7−36	10−38	14−40	18−51	23−45	35−44
2−37	5−21	7−37	10−39	14−41	19−27	24−40	35−45
2−39	5−26	7−40	10−40	14−42	19−33	24−45	36−45
2−40	5−27	7−41	10−41	14−44	19−42	24−54 Phe	36−48 Phe
2−41	5−28	7−42	10−44	14−45	19−45	25−42	38−48 Phe
2−42	5−35	7−44	10−46 Phe	14−47	19−55 Phe	26−47 Phe	38−52 Phe
2−45	5−38	7−53 Phe	10−55	15−22	20−29	26−53 Phe	39−49 Phe
2−47 Phe	5−39	8−15	11−21	15−35	20−30	27−35	39−50 Phe
2−49 Phe	5−40	8−16	11−28	15−37	20−34	27−38	40−50 Phe
3PG−10	5−41	8−23	11−43	15−39	20−35	27−40	41−51 Phe
3PG−11	5−42	8−26	11−44	15−40	20−36	27−42	42−52 Phe
3PG−12	5−43	8−27	11−45	15−44	20−37	27−47 Phe	43−53 Phe
3PG−15	5−44	8−31	11−47 Phe	15−53 Phe	20−39	28−37	46−53 Phe
3−18	5−46 Phe	8−35	11−52 Phe	16−24	20−40	28−39	
3−26	5−55 Phe	8−37	11PG−28	16−29	20−42	28−41	
3−28	6−13	8−38	11PG−29	16−36	20−43	28−43	

[a] Phe designates valine to phenylalanine mutation at position 46 (Aβ notation); PG = pyroglutamy.

dissolve in a 3% SDS solution as demonstrated by 4 h of centrifugation at 250000*g*, which generates only a comparatively minute pellet made of thioflavin-S-negative amorphous material. The differences in solubility between the species may be due to the greater age of the fibrillar amyloid in the cores of the AD deposits, relative to the mouse deposits, which permits a larger accumulation of post-translational modifications that hinder enzymatic hydrolysis (*34*). The complexity of the human plaque cores in terms of more abundant and diverse glycolipid- and glycoprotein-associated molecules may also hamper access to water and increase tertiary and quaternary structure stability.

It is interesting that human sporadic AD APP processing is strikingly different from that of the TgCRND8 Tg mice. The mice lacked the 9−11 kDa human SDS−PAGE bands corresponding to CT99 and CT83 species but did exhibit prominent 5 and 7 kDa bands that were not observed in sporadic human AD cases or ND control subjects. This altered APP processing pattern was reminiscent of that of PDAPP Tg mice expressing the Indiana mutation V717F (*4*) and may be the result of the sudden and elevated production of the mutant APP transcription, which simply overwhelms the capacity of the endogenous mouse secretase-processing enzymes. However, these proteolytic alterations may also be the result of the human APP mutation expressed in the Tg mice. These novel APP CT peptides encompassed the sequences of residues 43/44−99 (sequences given in the Aβ notation), which correspond to the CT55/56 amino acids of APP, and residues 52/53−99 (CT47/48), as suggested by MALDI-TOF and SELDI-TOF mass spectrometry. In sporadic AD as well as in APP23 and tg2576 mice, the peptides CT99 and CT83 represent the products of the β- and α-secretases from which the Aβ 40−42 and P3 (Aβ17−42) peptides are derived. The PDAPP Tg mice, on the other hand, hydrolyzed APP in the area of the cytosolic Lys−Lys−Lys residues (residues 53−54−55, Aβ notation) (*4*), rather than forming CT99 and CT83.

In the recently characterized familial AD PS V261I mutation (*23*), there was no evidence of shorter APP CT peptides. The processing of APP appears to be similar to that observed for sporadic AD. However, this PS mutation generates a peculiar class of plaques (cotton wool plaques) that are very abundant, homogeneous in appearance, and stained very faintly with thioflavin-S. Chemical characterization indicated that these plaques are mainly composed of N-terminally truncated Aβ species: 3−42/43 and 11−42/43. Apparently the absence of N-terminal amino acid residues imposes some constraints in the Aβ molecular structure that prevent the formation of the classical amyloid core plaques seen in sporadic AD. The PDAPP transgenic mice carrying the APP V717F mutation have negligible quantities of CT99 and CT83 but have an abundant quantity of shorter CTs (*4*). Intriguingly, the human FAD APP V717F mutation that produces longer Aβ peptides did not show shorter CT

peptides, but evidenced the human CT99 and CT83. The generation of shorter APP CT peptides appears to be a characteristic of the transgenic mouse species.

Whether the hydrolysis at sites adjacent to the surface of the cytosolic leaflet of the membrane bilayer is actually executed by the γ-secretase or by other cytosolic (trypsin-like) enzyme(s) remains to be established. However, production of Aβ and that of the APP intracellular domain (AICD) are apparently independent of each other, suggesting different γ-secretase activities or cofactors or different membrane environments that may account for this selectivity (*7*). It is also possible that the assortment of Aβ-related peptides with C-termini at residues 43, 44, 45, 46, 47, 48, 49, 50, 51, 52, and 53 (Aβ notation) in the PDAPP and TgCRND8 Tg mice are all generated by the γ-secretase as a consequence of the Val to Phe mutation at position 46 (Aβ notation). The bulky phenyl ring may alter the recognition consensus sequence of the γ-secretase and open new sites of hydrolysis other than the usual ϵ-, ζ-, or γ-sites (*40, 42*). On the other hand, these peptides may also be created by other carboxy- or endopeptidases. Amyloid-β peptides with C-termini extending beyond residues 40−42 have been observed in human skeletal muscle (*16*) and in humans expressing the Indiana FAD V717F mutation (*32*). Manipulations of APP by γ-secretase inhibitors (*41*), Phe-scanning mutagenesis of the APP transmembrane domain (*20*), or treatment with cathepsin-D (*9*) have also generated aberrant longer Aβ peptides. Another interesting question regarding the presence of shorter APP CT fragments (CT55/56 and CT47/48) in the TgCRND8 Tg mice is the sequence of enzymatic cleavage. In ND individuals as well as in sporadic and familial cases of AD, the β-secretase and the α-secretase cut first, generating CT99 and CT83, followed by the γ-secretase to create Aβ and P3 (*38*). Since in the TgCRND8 Tg mice SDS−PAGE demonstrates a total lack of the C-terminal peptides CT99 and CT83 and the presence of CT55/56 and CT47/48, which are sites closer to γ- and ϵ-cleavage sites, then one can argue that γ-secretase operates first and the β- and α-secretases subsequently generate the Aβ and the P3 fragments, respectively.

A crucial question surrounds the aftermath of altered proteolysis of APP transmembrane peptide domains: how are these remnants extruded and cleared from the membrane after hydrolysis? If these peptides are cleaved at the center of the transmembrane region, they could be driven out of the membrane by their respective ecto- and endodomains. However, longer Aβ peptides which span the whole membrane lipid bilayer and are thermodynamically stable in a nonpolar environment (i.e., the Aβ-related peptides ending at position 51 or 52) in the absence of further hydrolysis may be retained, thus altering membrane and cellular homeostasis as proposed by Marchesi (*21*). At this point it should be stated that the longer Aβ peptides that we found were detected in brain homogenates submitted to total lysis in the presence of concentrated GDFA. Hence, longer membrane retained Aβ peptides would become available to FPLC and HPLC separation technologies since the treatment with GDFA followed by centrifugation totally disrupted and eliminated membrane lipids. In support of this tenet is the observation that membrane rafts obtained under relatively mild experimental conditions are rich in retained dimeric Aβ and contained APP, secretases, Apo E, and the NFT protein tau (*12*). These membrane-bound peptides and proteins may end ultimately as the abundant autophagic bodies represented by degenerated multilamellar bodies and dense bodies observed in dystrophic neurites adjacent to amyloid core plaques (*26, 33*) in both AD and Tg mice (*22*).

As a result of the veritable amyloid production tidal wave in the TgCRND8 Tg mice that completely overwhelms the Aβ degradative capacity, an excess of these molecules accumulates in the vessel walls. Evidence suggests that amyloid plaque formation in Tg mice and AD initiates at the vessel walls (*24*, *25*, *35*) and that cerebrovascular damage may be an early event in amyloid pathology. This phenomenon may occur in the APP23 Tg mice in which early and sustained levels of soluble Aβ in the brain result in an accelerated and severe deposition of amyloid around the blood vessels (*13*). By contrast, in the tg2576 Tg mice the soluble amyloid appears to be efficiently eliminated from the brain through the general circulation, up to 8 months of age, resulting in a comparatively delayed and henceforth milder cerebrovascular amyloidosis (*14*).

The deposition of parenchymal and vascular amyloid in the TgCRND8 Tg mice at a younger age allows longer assessment of therapeutic interventions in a more aggressive model of brain amyloidosis. However, the initial vigor and immunologic integrity of the younger mice may play an important role in the efficient clearance of Aβ deposits, a situation not encountered in older Tg mouse models or in AD patients. The TgCRND8 Tg mouse model suggests that a rapid and abundant synthesis of soluble Aβ-related peptides is efficiently managed by their conversion into insoluble aggregates, whether fibrillar or floccular, thus emulating in a short period of time the longer human brain response. This physicochemical Aβ conversion also advocates that localized aggregation may be a mechanism of defense. An important aspect of the Tg mouse model is that the sudden and overwhelming Aβ production by far overcomes the enzymatic degradative machinery of the rodent's brain and its ability to clear the Aβ into the circulation. The TgCRND8 Tg mouse model demonstrates that survival is compatible, for most of the life span of these rodents, with an impressive load of Aβ deposition that forcefully invades all corners of the cerebrum and cerebellum, including the white matter. Active Aβ immunotherapy, in the younger TgCRND8 Tg mouse paradigm, is notably efficient in preventing and removing Aβ assemblies and apparently in averting memory deficits (*10*). However, a significant decrease in the total pool of Aβ, as detected by formic acid extraction of Aβ and ELISA immunoassays, is not observed in the TgCRND8 (*10*) and several other immunized Tg mouse models and immunized AD patients (*28*), suggesting that a pool of dimeric/oligomeric Aβ is still present in the brain. Whether this putatively "soluble" Aβ pool is present in the brain's extracellular space or associated with plasma or cytomembranes or more specifically with myelin remains to be determined. At least part of the immunization-mediated "disassembled" Aβ peptides appear to be undesirably associated with vascular amyloid deposits in an attempt to clear Aβ via the periarterial spaces (*28*). The long-term consequences of this Aβ vascular relocation may result in a more dysfunctional blood−brain barrier, increased vascular fragility, leading to bleeding episodes, and increased clogging of

periarterial spaces, compromising the removal of interstitial fluid.

In conclusion, the TgCRND8 Tg mice generate two basic types of Aβ peptides in response to the Swedish mutations and the Indiana mutation that aggregate into amyloid plaque cores and diffuse floccular deposits, respectively. The model also deposits a moderate amount of vascular amyloid that becomes more abundant as the mice age. The Swedish mutations appear to be responsible for the elevated production of Aβ ending at residues 40−42/43 and the Indiana mutation for the elongated forms of Aβ terminating at residues 52/53. These tenets are supported by the biochemical characterization of the Aβ peptides in the tg2576 and APP23 Tg mice that carry the Swedish mutations alone (*11*, *17*) and by the PDAPP Tg mice and familial Alzheimer's disease that carry the Indiana mutation (*4*, *32*). Elongated Aβ peptides may be in part responsible for the V717F Indiana familial Alzheimer's disease severity, its early onset, and premature death in the fifth decade of life. Our studies also suggest that the TgCRND8 Tg mice are a useful model for amyloid deposition insofar that they accumulate large quantities of Aβ peptides in a short period of time that appear to be partially removed by immunization and other therapeutic agents. Although the TgCRND8 mice are not a perfect phenocopy of sporadic AD, nevertheless they fulfill a pragmatic utilitarian role, although with limitations, given the biochemical differences in Aβ synthesis, biochemistry, and catabolism. The TgCRND8 Tg mice like other models that attempt to mimic AD amyloidosis are actually paradigms of the familial forms of this dementia, since all result from APP and PS mutations driven by powerful promoters and therefore do not duplicate sporadic AD. The failure to reproduce sporadic-type AD amyloidosis in animal models in the absence of APP and PS mutations strongly suggests that although Aβ is preeminent in AD, other important biochemical and physiological events related to the aging process influence Aβ deposition. Thus, as one muses the potential therapeutic effects of anti-Aβ immunization, inhibition of Aβ production, and enhanced Aβ degradation in the TgCRND8 Tg mice, cautious interpretation should be borne in mind in attempting to extrapolate the observations to humans.

ACKNOWLEDGMENT

We thank Dr. Samuel Gandy for the 369 antibody.

SUPPORTING INFORMATION AVAILABLE

A complete mass spectrometry data sheet of all 531 peptide species including the peptide fragment, post-translational modifications (when present), and the M_r-associated chromatographic peak and relative intensity. This material is available free of charge via the Internet at http://pubs.acs.org.

REFERENCES

1. Brookmeyer, R., Gray, S., and Kawas, C. (1998) Projections of Alzheimer's disease in the United States and the public health impact of delaying disease onset, *Am. J. Public Health 88* (9), 1337−1342.
2. Casas, C., Sergeant, N., Itier, J. M., Blanchard, V., Wirths, O., van der Kolk, N., Vingtdeux, V., van de Steeg, E., Ret, G., Canton, T., Drobecq, H., Clark, A., Bonici, B., Delacourte, A., Benavides, J., Schmitz, C., Tremp, G., Bayer, T. A., Benoit, P., and Pradier, L. (2004) Massive CA1/2 neuronal loss with intraneuronal and N-terminal truncated Abeta42 accumulation in a novel Alzheimer transgenic model, *Am. J Pathol. 165* (4), 1289−1300.
3. Chishti, M. A., Yang, D. S., Janus, C., Phinney, A. L., Horne, P., Pearson, J., Strome, R., Zuker, N., Loukides, J., French, J., Turner, S., Lozza, G., Grilli, M., Kunicki, S., Morissette, C., Paquette, J., Gervais, F., Bergeron, C., Fraser, P. E., Carlson, G. A., George-Hyslop, P. S., and Westaway, D. (2001) Early-onset amyloid deposition and cognitive deficits in transgenic mice expressing a double mutant form of amyloid precursor protein 695, *J. Biol. Chem. 276* (24), 21562−21570.
4. Esh, C., Patton, L., Kalback, W., Kokjohn, T. A., Lopez, J., Brune, D., Newell, A. J., Beach, T., Schenk, D., Games, D., Paul, S., Bales, K., Ghetti, B., Castano, E. M., and Roher, A. E. (2005) Altered APP Processing in PDAPP (Val717 → Phe) Transgenic Mice Yields Extended-Length Abeta Peptides, *Biochemistry 44* (42), 13807−13819.
5. Gelinas, D. S., Dasilva, K., Fenili, D., George-Hyslop, P., and McLaurin, J. (2004) Immunotherapy for Alzheimer's disease, *Proc. Natl. Acad. Sci. U.S.A. 101* (Suppl. 2), 14657−14662.
6. Hardy, J. A. and Higgins, G. A. (1992) Alzheimer's disease: the amyloid cascade hypothesis, *Science 256* (5054), 184−185.
7. Hecimovic, S., Wang, J., Dolios, G., Martinez, M., Wang, R., and Goate, A. M. (2004) Mutations in APP have independent effects on Abeta and CTFgamma generation, *Neurobiol. Dis. 17* (2), 205−218.
8. Heininger, K. (2000) A unifying hypothesis of Alzheimer's disease. IV. Causation and sequence of events, *Rev. Neurosci. 11* (Spec No.), 213−328.
9. Higaki, J., Catalano, R., Guzzetta, A. W., Quon, D., Nave, J. F., Tarnus, C., D'Orchymont, H., and Cordell, B. (1996) Processing of β-amyloid precursor protein by cathepsin D, *J. Biol. Chem. 271* (50), 31885−31893.
10. Janus, C., Pearson, J., McLaurin, J., Mathews, P. M., Jiang, Y., Schmidt, S. D., Chishti, M. A., Horne, P., Heslin, D., French, J., Mount, H. T., Nixon, R. A., Mercken, M., Bergeron, C., Fraser, P. E., George-Hyslop, P., and Westaway, D. (2000) Aβ peptide immunization reduces behavioural impairment and plaques in a model of Alzheimer's disease, *Nature 408* (6815), 979−982.
11. Kalback, W., Watson, M. D., Kokjohn, T. A., Kuo, Y. M., Weiss, N., Luehrs, D. C., Lopez, J., Brune, D., Sisodia, S. S., Staufenbiel, M., Emmerling, M., and Roher, A. E. (2002) APP transgenic mice Tg2576 accumulate Aβ peptides that are distinct from the chemically modified and insoluble peptides deposited in Alzheimer's disease senile plaques, *Biochemistry 41* (3), 922−928.
12. Kawarabayashi, T., Shoji, M., Younkin, L. H., Wen-Lang, L., Dickson, D. W., Murakami, T., Matsubara, E., Abe, K., Ashe, K. H., and Younkin, S. G. (2004) Dimeric amyloid β protein rapidly accumulates in lipid rafts followed by apolipoprotein E and phosphorylated tau accumulation in the Tg2576 mouse model of Alzheimer's disease, *J. Neurosci. 24* (15), 3801−3809.
13. Kuo, Y. M., Beach, T. G., Sue, L. I., Scott, S., Layne, K. J., Kokjohn, T. A., Kalback, W. M., Luehrs, D. C., Vishnivetskaya, T. A., Abramowski, D., Sturchler-Pierrat, C., Staufenbiel, M., Weller, R. O., and Roher, A. E. (2001) The evolution of A beta peptide burden in the APP23 transgenic mice: implications for A beta deposition in Alzheimer disease, *Mol. Med. 7* (9), 609−618.
14. Kuo, Y. M., Crawford, F., Mullan, M., Kokjohn, T. A., Emmerling, M. R., Weller, R. O., and Roher, A. E. (2000) Elevated Aβ and apolipoprotein E in AβPP transgenic mice and its relationship to amyloid accumulation in Alzheimer's disease, *Mol. Med. 6* (5), 430−439.
15. Kuo, Y. M., Emmerling, M. R., Vigo-Pelfrey, C., Kasunic, T. C., Kirkpatrick, J. B., Murdoch, G. H., Ball, M. J., and Roher, A. E. (1996) Water-soluble Abeta (N-40, N-42) oligomers in normal and Alzheimer disease brains, *J. Biol. Chem. 271* (8), 4077−4081.
16. Kuo, Y. M., Kokjohn, A., Watson, M. D., Woods, A. S., Cotter, R. J., Sue, L. I., Kalback, W. M., Emmerling, M. R., Beach, T. G., and Roher, A. E. (2000) Elevated Aβ42 in skeletal muscle of Alzheimer disease patients suggests peripheral alterations of AβPP metabolism, *Am. J. Pathol. 156* (3), 797−805.
17. Kuo, Y. M., Kokjohn, T. A., Beach, T. G., Sue, L. I., Brune, D., Lopez, J. C., Kalback, W. M., Abramowski, D., Sturchler-Pierrat, C., Staufenbiel, M., and Roher, A. E. (2001) Comparative analysis of amyloid-beta chemical structure and amyloid plaque morphology of transgenic mouse and Alzheimer's disease brains, *J. Biol. Chem. 276* (16), 12991−12998.

18. Kurt, M. A., Davies, D. C., Kidd, M., Duff, K., Rolph, S. C., Jennings, K. H., and Howlett, D. R. (2001) Neurodegenerative changes associated with beta-amyloid deposition in the brains of mice carrying mutant amyloid precursor protein and mutant presenilin-1 transgenes, *Exp. Neurol. 171* (1), 59−71.
19. Lee, P. H., Hwang, E. M., Hong, H. S., Boo, J. H., Mook-Jung, I., and Huh, K. (2006) Effect of ischemic neuronal insults on amyloid precursor protein processing, *Neurochem. Res. 31* (6), 821−827.
20. Lichtenthaler, S. F., Wang, R., Grimm, H., Uljon, S. N., Masters, C. L., and Beyreuther, K. (1999) Mechanism of the cleavage specificity of Alzheimer's disease gamma-secretase identified by phenylalanine-scanning mutagenesis of the transmembrane domain of the amyloid precursor protein, *Proc. Natl. Acad. Sci U.S.A. 96* (6), 3053−3058.
21. Marchesi, V. T. (2005) An alternative interpretation of the amyloid Abeta hypothesis with regard to the pathogenesis of Alzheimer's disease, *Proc. Natl. Acad. Sci. U.S.A. 102* (26), 9093−9098.
22. Masliah, E., Sisk, A., Mallory, M., Mucke, L., Schenk, D., and Games, D. (1996) Comparison of neurodegenerative pathology in transgenic mice overexpressing V717F beta-amyloid precursor protein and Alzheimer's disease, *J. Neurosci. 16* (18), 5795−5811.
23. Miravalle, L., Calero, M., Takao, M., Roher, A. E., Ghetti, B., and Vidal, R. (2005) Amino-terminally truncated Abeta peptide species are the main component of cotton wool plaques, *Biochemistry 44* (32), 10810−10821.
24. Miyakawa, T., Shikai, I., Shimoji, A., Kuramoto, R., and Nagatoshi, K. (1979) Electron-microscopical study on senile plaques in Alzheimer's disease, *Folia Psychiatr. Neurol. Jpn. 33* (2), 197−203.
25. Miyakawa, T., and Uehara, Y. (1979) Observations of amyloid angiopathy and senile plaques by the scanning electron microscope, *Acta Neuropathol. 48* (2), 153−156.
26. Nixon, R. A., Wegiel, J., Kumar, A., Yu, W. H., Peterhoff, C., Cataldo, A., and Cuervo, A. M. (2005) Extensive involvement of autophagy in Alzheimer disease: an immuno-electron microscopy study, *J. Neuropathol. Exp. Neurol. 64* (2), 113−122.
27. Oddo, S., Caccamo, A., Shepherd, J. D., Murphy, M. P., Golde, T. E., Kayed, R., Metherate, R., Mattson, M. P., Akbari, Y., and LaFerla, F. M. (2003) Triple-transgenic model of Alzheimer's disease with plaques and tangles: intracellular Abeta and synaptic dysfunction, *Neuron 39* (3), 409−421.
28. Patton, R. L., Kalback, W. M., Esh, C. L., Kokjohn, T. A., Van Vickle, G. D., Luehrs, D. C., Kuo, Y. M., Lopez, J., Brune, D., Ferrer, I., Masliah, E., Newel, A. J., Beach, T. G., Castano, E. M., and Roher, A. E. (2006) Amyloid-beta peptide remnants in AN-1792-immunized Alzheimer's disease patients: a biochemical analysis, *Am. J. Pathol. 169* (3), 1048−1063.
29. Pearson, H. A., and Peers, C. (2006) Physiological roles for amyloid beta peptides, *J. Physiol. 575* (Pt 1), 5−10.
30. Roher, A. E., Chaney, M. O., Kuo, Y. M., Webster, S. D., Stine, W. B., Haverkamp, L. J., Woods, A. S., Cotter, R. J., Tuohy, J. M., Krafft, G. A., Bonnell, B. S., and Emmerling, M. R. (1996) Morphology and toxicity of Abeta-(1−42) dimer derived from neuritic and vascular amyloid deposits of Alzheimer's disease, *J. Biol. Chem. 271* (34), 20631−20635.
31. Roher, A. E., Kokjohn, T. A., and Beach, T. G. (2006) An association with great implications: vascular pathology and Alzheimer disease, *Alzheimer Dis. Assoc. Disord. 20* (1), 73−75.
32. Roher, A. E., Kokjohn, T. A., Esh, C., Weiss, N., Childress, J., Kalback, W., Luehrs, D. C., Lopez, J., Brune, D., Kuo, Y. M., Farlow, M., Murrell, J., Vidal, R., and Ghetti, B. (2004) The human amyloid-β precursor protein$_{770}$ mutation 717 val-phe generates peptides longer than Aβ 40−42 and flocculent amyloid aggregates, *J. Biol. Chem. 279* (7), 5829−5836.
33. Roher, A. E., Kuo, Y. M., Kokjohn, T. A., Emmerling, M. R., and Gracon, S. (1999) Amyloid and lipids in the pathology of Alzheimer disease, *Amyloid 6* (2), 136−145.
34. Roher, A. E., Lowenson, J. D., Clarke, S., Wolkow, C., Wang, R., Cotter, R. J., Reardon, I. M., Zurcher-Neely, H. A., Heinrikson, R. L., Ball, M. J., and Greenberg, B. D. (1993) Structural alterations in the peptide backbone of beta-amyloid core protein may account for its deposition and stability in Alzheimer's disease, *J. Biol. Chem. 268* (5), 3072−3083.
35. Roher, A. E., Lowenson, J. D., Clarke, S., Woods, A. S., Cotter, R. J., Gowing, E., and Ball, M. J. (1993) beta-Amyloid-(1−42) is a major component of cerebrovascular amyloid deposits: implications for the pathology of Alzheimer disease, *Proc. Natl. Acad. Sci. U.S.A. 90* (22), 10836−10840.
36. Roher, A. E., Palmer, K. C., Yurewicz, E. C., Ball, M. J., and Greenberg, B. D. (1993) Morphological and biochemical analyses of amyloid plaque core proteins purified from Alzheimer disease brain tissue, *J. Neurochem. 61*(5), 1916−1926.
37. Schenk, D., Barbour, R., Dunn, W., Gordon, G., Grajeda, H., Guido, T., Hu, K., Huang, J., Johnson-Wood, K., Khan, K., Kholodenko, D., Lee, M., Liao, Z., Lieberburg, I., Motter, R., Mutter, L., Soriano, F., Shopp, G., Vasquez, N., Vandevert, C., Walker, S., Wogulis, M., Yednock, T., Games, D., and Seubert, P. (1999) Immmunization with amyloid-β attenuates Alzheimer-disease-like pathology in the PDAPP mouse, *Nature 400* (6740), 173−177.
38. Selkoe, D. J. (2001) Alzheimer's disease: Genes, proteins, and therapy, *Physiol. Rev. 81* (2), 741−766.
39. Watson, D., Castano, E., Kokjohn, T. A., Kuo, Y. M., Lyubchenko, Y., Pinsky, D., Connolly, E. S., Jr., Esh, C., Luehrs, D. C., Stine, W. B., Rowse, L. M., Emmerling, M. R., and Roher, A. E. (2005) Physicochemical characteristics of soluble oligomeric Abeta and their pathologic role in Alzheimer's disease, *Neurol. Res. 27* (8), 869−881.
40. Weidemann, A., Eggert, S., Reinhard, F. B., Vogel, M., Paliga, K., Baier, G., Masters, C. L., Beyreuther, K., and Evin, G. (2002) A novel epsilon-cleavage within the transmembrane domain of the Alzheimer amyloid precursor protein demonstrates homology with Notch processing, *Biochemistry 41* (8), 2825−2835.
41. Yagishita, S., Morishima-Kawashima, M., Tanimura, Y., Ishiura, S., and Ihara, Y. (2006) DAPT-induced intracellular accumulations of longer amyloid beta-proteins: further implications for the mechanism of intramembrane cleavage by gamma-secretase, *Biochemistry 45* (12), 3952−3960.
42. Zhao, G., Mao, G., Tan, J., Dong, Y., Cui, M. Z., Kim, S. H., and Xu, X. (2004) Identification of a new presenilin-dependent zeta-cleavage site within the transmembrane domain of amyloid precursor protein, *J. Biol. Chem. 279* (49), 50647−50650.

BI700951U